NANO · MICRO small
www.small-journal.com

# A Dual-Cross-Linked Hydrogel Patch for Promoting Diabetic Wound Healing

*Jing Liu, Moyuan Qu, Canran Wang, Yumeng Xue, Hui Huang, Qianming Chen, Wujin Sun, Xingwu Zhou,* Guihua Xu,* and Xing Jiang**

**Diabetic wound treatment faces significant challenges in clinical settings. Alternative treatment approaches are needed. Continuous bleeding, disordered inflammatory regulation, obstruction of cell proliferation, and disturbance of tissue remodeling are the main characteristics of diabetic wound healing. Hydrogels made of either naturally derived or synthetic materials can potentially be designed with a variety of functions for managing the healing process of chronic wounds. Here, a hemostatic and anti-inflammatory hydrogel patch is designed for promoting diabetic wound healing. The hydrogel patch is derived from dual-cross-linked methacryloyl-substituted *Bletilla Striata* polysaccharide (B) and gelatin (G) via ultraviolet (UV) light. It is demonstrated that the B–G hydrogel can effectively regulate the M1/M2 phenotype of macrophages, significantly promote the proliferation and migration of fibroblasts in vitro, and accelerate angiogenesis. It can boost wound closure by normalizing epidermal tissue regeneration and depositing collagen appropriately in vivo without exogenous cytokine supplementation. Overall, the B–G bioactive hydrogel can promote diabetic wound healing in a simple, economical, effective, and safe manner.**

## 1. Introduction

The management of diabetic wounds has become a significant challenge to the global health care system and seriously affected patients' quality of life.[1] The normal healing process (hemostasis, inflammation, proliferation, and tissue remodeling) is severely impaired in the scenario of chronic wounds. Disorder of these physiological processes causes persistent inflammation and dysfunctional epithelial formation. Eventually, it leads to wound nonunion and increases the risk of infection.[2] Accumulating evidence indicates that for accelerating diabetic wound healing, it is crucial to avoid excessive inflammation, including secretion of inflammatory factors in chronic wounds and inappropriate macrophage differentiation.[3] The classically activated macrophages (M1) and alternatively activated macrophages (M2) are two typical phenotypes of macrophages.[4] The M1 phenotype macrophages in diabetic wounds continue to release pro-inflammatory cytokines, such as tumor necrosis factor alpha (TNF-$\alpha$), which stimulate apoptosis of cells (fibroblasts, keratinocytes, and endothelial cells) and disorder collagen deposition, while M2 macrophages can accelerate fibroblast proliferation, orchestrate anti-inflammatory responses, stabilize angiogenesis, and promote extracellular matrices (ECM) remodeling.[5] The ineffective transition of macrophages from M1 to M2 phenotype can lead to wound nonunion or scar formation.[6] Therefore, inducing the anti-inflammatory transformation of macrophages could be a promising approach for developing clinical treatment of diabetic wounds.

J. Liu, H. Huang, G. Xu, X. Jiang
School of Nursing
Nanjing University of Chinese Medicine
Nanjing 210023, China
E-mail: guihua.xu@njucm.edu.cn; jiangxing@njucm.edu.cn

M. Qu, Q. Chen
Stomatology Hospital
School of Stomatology
Zhejiang University School of Medicine
Zhejiang Provincial Clinical Research Center for Oral Diseases
Key Laboratory of Oral Biomedical Research of Zhejiang Province
Cancer Center of Zhejiang University
Hangzhou 310006, China

The ORCID identification number(s) for the author(s) of this article can be found under https://doi.org/10.1002/smll.202106172.

**DOI: 10.1002/smll.202106172**

C. Wang
School of Medicine
Shanghai Jiao Tong University
Shanghai 200025, China

Y. Xue
State Key Laboratory of Solidification Processing
Center for Nano Energy Materials
School of Materials Science and Engineering
Northwestern Polytechnical University
Xi'an 710072, China

W. Sun
Department of Biological Systems Engineering
Virginia Tech
Blacksburg, VA 24061, USA

X. Zhou
Department of Pharmaceutical Sciences
University of Michigan
Ann Arbor, MI 48105, USA
E-mail: xwzhou@med.umich.edu

 

A well-designed hydrogel could be an excellent platform for promoting chronic wound healing. Hydrogel scaffold can affect the phenotypes of cells. Feng et al.[7] designed a novel bio-inspired glycopeptide hydrogel that can regulate macrophage polarization and promote angiogenesis, thereby accelerating wound healing without requiring any additional therapeutic drugs. Another macrophage-activating hydrogel system containing two bioactive polysaccharides (konjac glucomannan and heparin) was also reported.[8] The researchers aimed to harness endogenous growth factors for inducing blood vessel formation in vivo without the supplementation of any exogenous proteins. Therefore, selecting suitable hydrogel substrates could provide an anti-inflammatory scaffold with wound healing capabilities.

Recently, many studies have focused on developing natural polysaccharide-based biomaterials for diverse regenerative medicine and tissue engineering applications.[9] *Bletilla Striata* (*B. Striata*) polysaccharide (BSP) is a naturally derived polysaccharide that can induce wound healing (hemostasis, anti-inflammation, promoting blood vessels, cell proliferation, and migration).[10] BSP is a type of glucomannan, which has D-mannose and D-glucose in its backbone, and it is affinitive to macrophages through mannose receptors (MR).[11] Such interactions can induce the expression of pro-angiogenic cytokines,[12] and BSP can also reduce the expression of pro-inflammatory cytokine TNF-α in diabetic wounds.[13] Besides that, BSP can inhibit angiotensin II or lipopolysaccharide (LPS)-induced pro-inflammatory cytokine interleukin-6 (IL-6) concentration[14] and activate transforming growth factor beta 1 (TGF-β1)/Smad2 pathway to promote collagen deposition.[15] However, the lack of cell adhesion capability limits its use as tissue scaffolds. Meanwhile, gelatin methacrylate (GelMA) contains arginine–glycine–aspartic acid (RGD) peptide sequence that could interact with cell integrin receptors. These interactions could promote cell adhesion and platelet (PLT) activation, which might give the hydrogel good cell adhesion property[16] and hemostatic promoting ability.[17] Interestingly, due to integrin-mediated interactions, THP-1 cells encapsulated in GelMA hydrogels showed increased interleukin-10 (IL-10) (M2-related cytokine) expression and reduced expression of IL-6, especially under inflammatory conditions.[18]

Here, we demonstrate an M1/M2 phenotype-based anti-inflammatory dual-cross-linked hydrogel (B–G) consisting of methacryloyl-substituted BSP (BSPMA) and GelMA (**Figure 1**A). Compared with a single network structure, the B–G hydrogel can be optimized for mechanical properties, degradation rate, and swelling rate while maintaining its capabilities for chronic wound healing. The composition and fabrication process of the composite hydrogel patch is optimized based on cell adhesion, proliferation, migration, and macrophages polarization assays in vitro. A diabetic full-thickness wound model has been used to evaluate the in vivo healing efficacy of the B–G hydrogel. This study demonstrates the potential of the dual-cross-linked B–G hydrogels with enhanced hemostatic, anti-inflammatory,

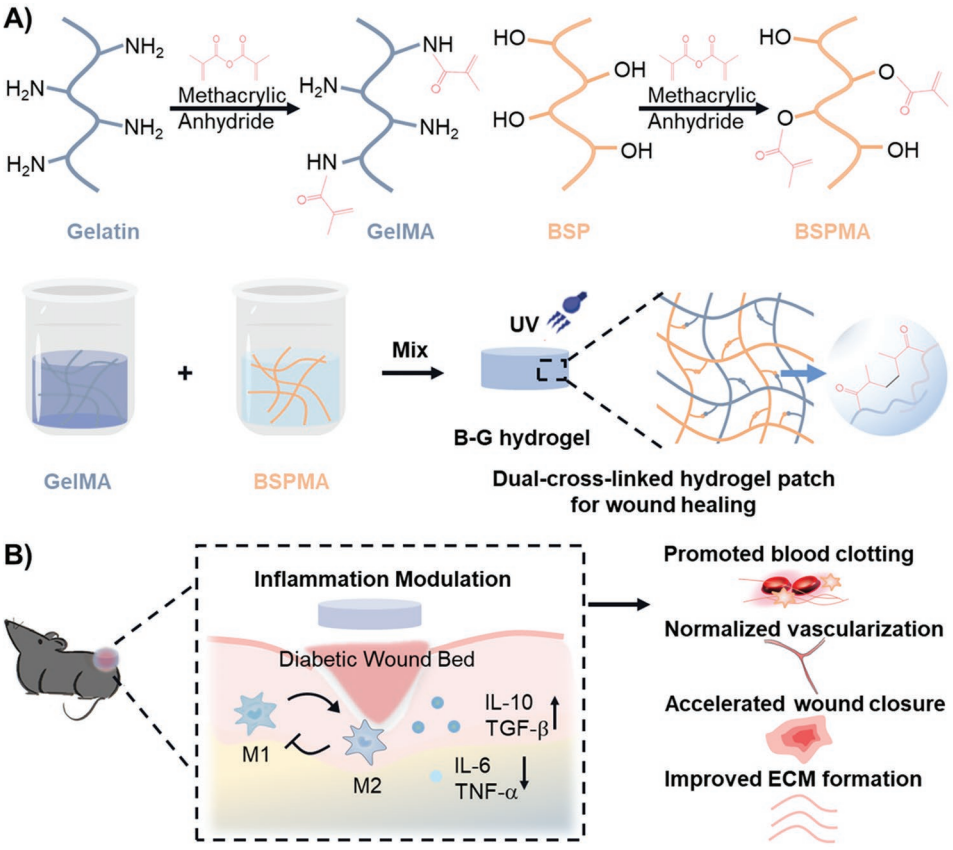


**Figure 1.** A) Schematic for preparing GelMA, BSPMA, and dual-cross-linked B–G hydrogel patch. B) Schematic illustration of mechanism of dual-cross-linked B–G hydrogel patch accelerates diabetic chronic wound healing.

effective wound closure capabilities for diabetic wound healing management (Figure 1B).

## 2. Results and Discussions

### 2.1. Fabrication and Characterization of BSPMA Hydrogel

Synthetic materials might be suboptimal to simulate a natural ECM.[19] Increasing attention has focused on repairing damaged tissue by engineering scaffolds based on naturally derived materials.[20] Natural polymers have a wide range of sources. BSP is the main active component of *B. Striata* with a defined molecular structure (Figure S1A, Supporting Information) and could be chemically modified for additional functions.[21] In this study, by incorporating reactive methacrylate groups into BSP (Mw = 51.4 kDa, Figure S1B, Supporting Information), a photo-cross-linkable BSP prepolymer (BSPMA) was synthesized. As shown in Figure S1C, Supporting Information, successful conjugation was confirmed by proton nuclear magnetic resonance ($^1$H-NMR) with the methacrylate peaks at 5.60 and 6.05 ppm (acrylic protons of methacrylamide groups), respectively. The degree of methacrylation of BSPMA is 57.3%, determined by comparing the intensity of the double bond region (5.60 and 6.05 ppm) to the methylene protons (1.80 ppm).[22] The appearance of BSPMA in solutions is shown in Figure S1D, Supporting Information. GelMA was synthesized from Gelatin (Mw = 80.8 kDa, Figure S1B,C, Supporting Information) and GelMA was used as another cross-linkable network to compensate for the lack of cell adhesion in polysaccharides.[23] The degree of methacrylation of GelMA is 64.9%, determined by comparing the intensity of the double bond region (5.40 ppm) to the aromatic protons (7.20 ppm).[24] By admixing the solution of GelMA and BSPMA, a dual-cross-linked B–G hydrogel patch could be formed through ultraviolet (UV) cross-linking (Figure S1E, Supporting Information).

### 2.2. Optimization of the Composition of B–G Hydrogel

10% GelMA has been shown to increase the adherence and growth of the cells.[25] In order to optimize the concentration of BSPMA, concentration gradients of BSPMA were added, and the cell viability was evaluated (Figure S2A, Supporting Information). Compared with other groups, 2% BSPMA and GelMA in combination have the best cell viability. Therefore, we selected 2% BSPMA and 10% GelMA as the final composition for further evaluation.

#### *2.2.1. Morphological Features of the Hydrogel*

The average pore size of a biological scaffold is a critical parameter affecting cell viability, attachment, and differentiation.[26] The 3D bulk structure of the B–G hydrogel was observed using scanning electron microscope (SEM). The hydrogel is highly porous with moderate thickening of the hole wall (**Figure 2**A). The average pore size was 85.20 ± 4.99 μm (Figure 2B) with 72.13 ± 2.15% porosity (Figure S2B, Supporting Information), which is beneficial for cell viability and wound healing.[26,27] The pore size of the B–G hydrogel was smaller than that of single network BSPMA (95.30 ± 6.64 μm) and GelMA (88.61 ± 4.30 μm), possibly due to the tight cross-linking of dual-network structure.

#### *2.2.2. Physicochemical Properties of the Hydrogel*

The mechanical properties of hydrogel can be readily adjusted by changing the UV irradiation time to meet the needs of different tissues.[16] In order to characterize the mechanical properties of B–G hydrogels with different cross-linking times, a compression test was performed on the samples under different cross-linking conditions of 5, 15, and 30 s, respectively. As shown in Figure 2C, the stress–strain curve showed that the stiffness improved with the increase of cross-linking time. The ultimate stress of B–G hydrogel increased significantly over time (31.49 kPa for 5 s B–G, 235.85 kPa for 15 s B–G, and 385.93 kPa for 30 s B–G). The higher cross-linking degree is beneficial to forming robust hydrogel, but it also displayed relatively brittle.[28] In order to obtain strong and elastic hydrogels, we chose the 15 s cross-linking time as the optimized condition. At the same cross-linking time, the compression modulus of B–G hydrogel (62.93 ± 8.24 kPa) was significantly higher than that of the individual component BSPMA (9.77 ± 1.84 kPa) and GelMA (17.63 ± 4.43 kPa) (Figure 2D,E). The structure of a dual-cross-linked hydrogel has improved mechanical properties compared to the single network. The resulting modulus of compression also lies within the range of physiological soft tissue (10–200 kPa),[29] which was favorable as a scaffold for cell proliferation, migration, and differentiation. The storage modulus $G'$ and the loss modulus $G''$ of the BSPMA, GelMA, and B–G hydrogels were also evaluated by rheological experiments.[30] Figure 2F shows the dynamic change graph. In the range of $\gamma = 10\%$ the storage modulus ($G'$) of all samples were higher than the loss modulus ($G''$) indicating the hydrogel formation. In addition, the storage modulus of the B–G hydrogel was higher than the corresponding single network hydrogel.

We further characterized the swelling rate of the hydrogel, which affected the water absorption of the wound exudate and the change of the scaffold volume. As shown in Figure 2G, GelMA reached swelling equilibrium (≈781%) in 480 min, while the swelling rate of BSPMA was higher than that of GelMA and B–G group ($p < 0.05$) in the first 10 min, and quickly reached the swelling equilibrium (≈435.5%) within 3 min, which was attributed to hydrogel's hydrophilic structure and high porosity. Interestingly, the B–G hydrogel also showed appropriate swelling ability, and the water absorption was continuously higher than that of GelMA ($p < 0.05$) when the pre-30 min reached the swelling equilibrium (≈511.3%). It was found that the B–G hydrogel can quickly absorb exudate and blood in the early stage and maintain a stable shape and volume while keeping a moist healing environment to avoid continuous compression to the surrounding fragile granulation tissue.

Type II collagenase (matrix metalloproteinase-8 [MMP-8]) is the main proteolytic enzyme involved in wound healing.[31] GelMA has been shown to be degraded by enzyme because gelatin contains a sequence that can be recognized by

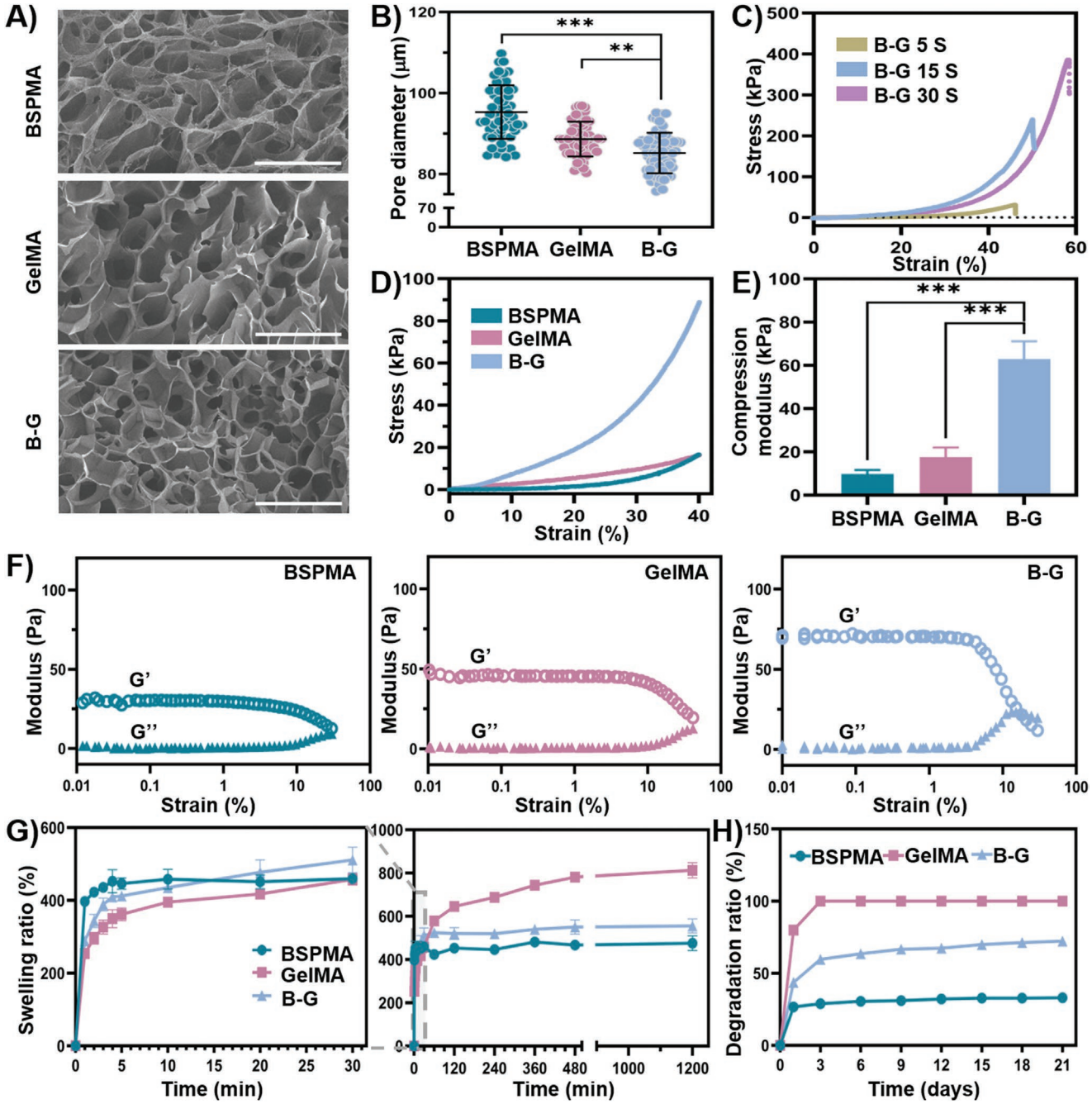


**Figure 2.** A) SEM of the cross section of the BSPMA, GelMA, and BSPMA-GelMA hydrogels (Scale bar = 250 μm). B) Pore size distribution of BSPMA, GelMA, and B–G hydrogel. C) Tensile stress–strain curves of B–G hydrogels after UV cross-linking for 5, 15, and 30 s. D) Compressive stress–strain characterization of BSPMA, GelMA, and B–G hydrogels. E) Compressive modulus of BSPMA, GelMA, and B–G hydrogels ($n = 3$). F) Storage and loss modulus of BSPMA, GelMA, and B–G hydrogels. G) Swelling ratio of BSPMA, GelMA, and B–G hydrogels in PBS (pH 7.4) ($n = 4$). H) Degradation ratio of BSPMA, GelMA and B–G hydrogels after 21 days of degradation ($n = 4$). Data represent mean ± SD; $^{**}p < 0.01$, $^{***}p < 0.001$.

collagenases.[32] To evaluate degradation, hydrogels were immersed in type II collagenase solution (1.25 U $mL^{-1}$). As shown in Figure 2H, BSPMA degraded slowly because of the lack of functional sequence. B–G hydrogel is considered to be more suitable for long-term wound healing. When incubated for 21 days, it degraded 72.14 ± 1.32%. Because BSPMA and GelMA are intertwined, the B–G hydrogel exhibits a slower degradation rate than GelMA.[33] Meanwhile, the inexistence of MMP-sensitive motifs in BSPMA makes B–G hydrogels immersed in the Type II collagenase solution take longer to degrade. The results showed that B–G hydrogel could exist in the wound bed for a long time with appropriate degradation capacity, maintain a moist healing environment to ensure optimal healing.

### 2.3. Polarization of Macrophages from M1 to M2 Phenotype

A prominent feature of macrophages during M1 or M2 polarization is the increased expression of CD86 or CD206.[7] In pathological wounds of diabetes mellitus, macrophages can hardly convert from pro-inflammatory M1 phenotype to pro-healing M2 phenotype, leading to an extended inflammatory state, limited angiogenesis, and delayed wound healing. Biological materials with specific physical and biochemical properties might be able to regulate their differentiation.[26,34]

RAW 264.7 cell line was used to assess the polarization efficacy of the hydrogel. After stimulated with LPS, RAW 264.7 cells were further treated with interleukin-4 (IL-4) (positive control), and different gels, respectively. Cell treated with LPS only were used as the negative control.[7,35] The level of macrophage transformation in different groups was detected by flow cytometry. After being stimulated by LPS, the proportion of $CD206^{+}CD86^{-}$ (M2) and $CD206^{-}CD86^{+}$ (M1) macrophages in the control group was 2.4% and 60.3%, respectively (**Figure 3**A). The cells were incubated with BSPMA, GelMA, and B–G hydrogel, respectively. The results showed that B–G hydrogel could effectively promote the phenotype transformation of macrophages from M1 to M2. In Figure 3B,C, the B–G group showed the best efficacy in promoting the macrophages transformation. Compared with the control group, the percentage of macrophages in the M1 phenotype decreased significantly in B–G group ($p < 0.001$). Since Arginase-1(ARG-1) is also a widely used marker of M2 macrophage,[36] the expression of ARG-1 in macrophages were observed by immunofluorescence staining after treatments, and the same trend was found (Figure 3D and Figure S2C, Supporting Information). TNF-α, IL-6, IL-10, and TGF-β levels were also evaluated by quantitative polymerase chain reaction (q-PCR), respectively. As presented in Figure 3E, compared with the control group, the mRNA expression of inflammatory TNF-α and IL-6 reduced significantly, whereas the mRNA expression of anti-inflammatory IL-10 and TGF-$\beta$ elevated in the cells treated with B–G gel.

As one type of plant-derived natural glucomannan, BSP has rich MR (c-type lectins and cell surface receptors) with a high affinity to macrophages,[11,21] which might contribute to

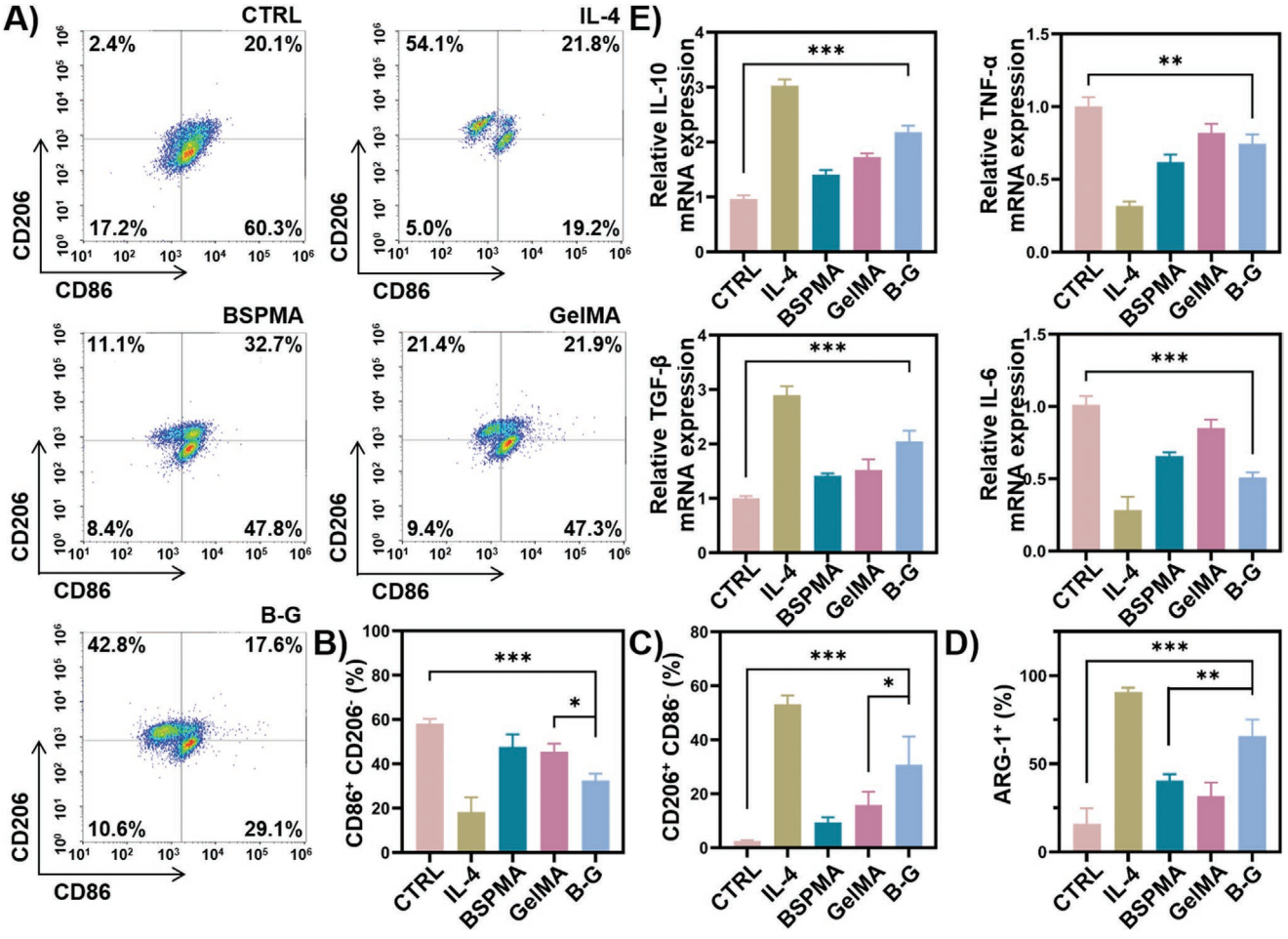


**Figure 3.** A) Flow cytometry analysis of CD206 and CD86 expression of RAW 264.7 cells treated with LPS (control), IL-4 (positive control), BSPMA, GelMA, and B–G hydrogel. Statistical histogram of B) M1 ($CD86^{+}$) or C) M2 ($CD206^{+}$) type macrophages ratio after treated with LPS (control), IL-4, BSPMA, GelMA, and B–G hydrogel ($n = 3$). D) Quantitative analysis of average fluorescent intensity of ARG-1 of RAW 264.7 cells treated with LPS (control), IL-4, BSPMA, GelMA, and B–G hydrogel ($n = 3$). E) Relative mRNA expression of IL-10, TGF-β, TNF-α, and IL-6 of RAW 264.7 cells treated with LPS (control), IL-4, BSPMA, GelMA, and B–G hydrogel ($n = 3$). Data represent mean ± SD; $^{*}p < 0.05$, $^{**}p < 0.01$, $^{***}p < 0.001$.

its functionality for macrophage phenotypes regulation. The appropriate healing immune environment is accompanied by producing anti-inflammatory cytokines.[5] The wound of diabetic mice was accompanied by an increase in the concentration of TNF-α, which accelerated the apoptosis of fibroblasts and delayed wound healing.[37] It has been proved that BSP regulates macrophages by inhibiting NLRP3 inflammatory bodies to promote diabetic inflammatory wound healing[13] and accelerate collagen deposition of dermal wounds in mice by TGF-β1/Smad2 pathway.[15] In addition, GelMA may regulate the decrease of TNF-α in the immune system under pro-inflammatory conditions or even reach a normal level[38] and increased M2-related cytokine IL-10 gene expression.[18]

### 2.4. Cell Proliferation, Migration, Biocompatibility, and Adhesion In Vitro

The interaction between cells and materials is essential in tissue engineering. Cell adhesion is the basis of communication between cells and the microenvironment and dictates cell migration, proliferation, differentiation, and other essential cell behaviors.[39] Due to the presence of cell adhesion and MMP reactive peptide group, GelMA has been widely used in wound healing. As shown in **Figure 4**A, after incubation in the medium for 4 h, NIH/3T3 cells efficiently attached to the GelMA and B–G hydrogels in similar behavior as on the TCP culture dishes, indicating that GelMA and B–G hydrogels could rapidly promote the adhesion of fibroblasts and disperse evenly, while BSPMA aggregates were significantly different from those in B–G group ($p < 0.05$) (Figure S2D, Supporting Information).

The CCK-8 assay was further applied to quantitatively detect the proliferation of NIH/3T3 cells cultivated with or without hydrogels. As shown in Figure 4B, cells cultured on the hydrogels presented excellent cell proliferation after being incubated for 1 day. For the B–G group, cells proliferated dramatically on day 3, after which cell proliferation continued in the later culture time and outperformed other groups. Similar results were also confirmed by Live/Dead staining (Figure 4C and Figure S2E, Supporting Information).

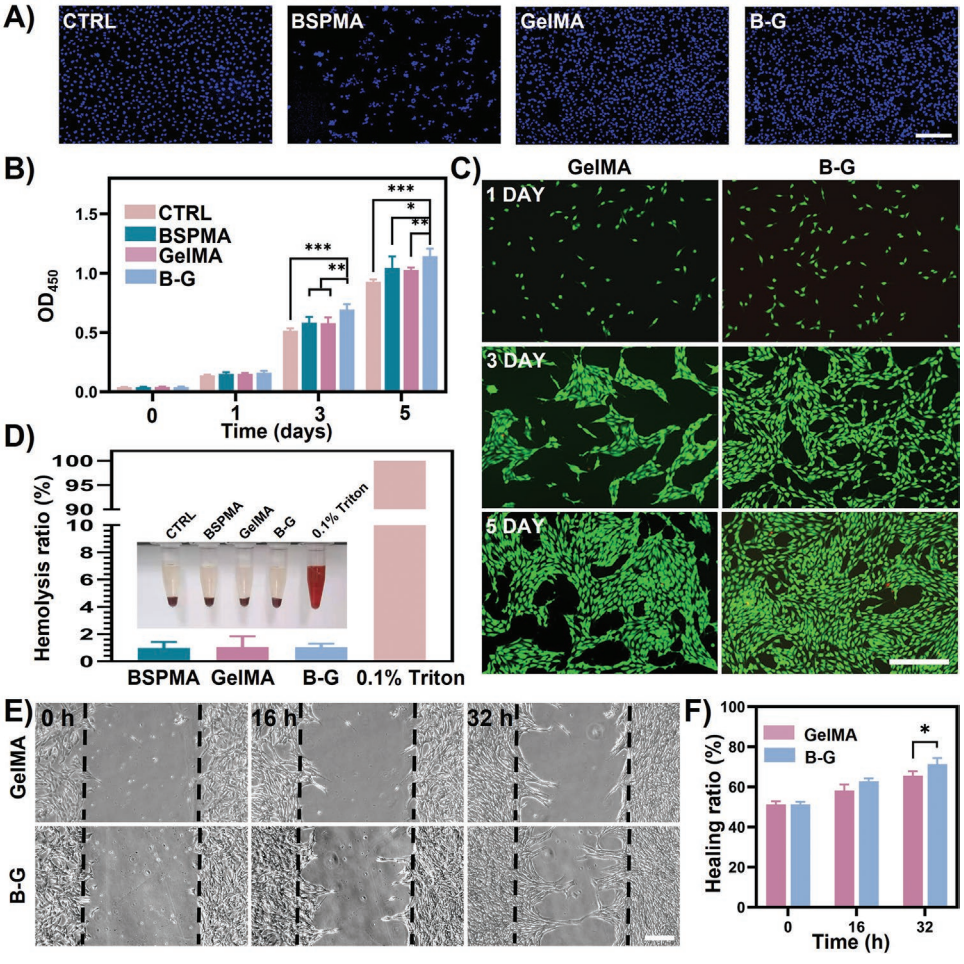


**Figure 4.** A) Cell adhesion on the surface of the control (TCP culture dishes), BSPMA, GelMA, and B–G hydrogel (Scale bar = 400 μm). B) Proliferation of NIH/3T3 incubated for 1, 3, and 5 days on control (TCP culture dishes), BSPMA, GelMA, and B–G ($n = 3$). C) Live/Dead staining of NIH/3T3 after culture on GelMA and B–G hydrogel for 1, 3, and 5 days (Scale bar = 300 μm). D) Hemolytic percentage of the control (0.9% NaCl solution), BSPMA, GelMA, B–G, and 0.1% Triton X-100 ($n = 3$). E) Images of wound scratch migration assay and F) Quantification of NIH/3T3 cells migration on GelMA and B–G hydrogel ($n = 3$) (Scale bar = 200 μm). Data represent mean ± SD; *$p < 0.05$, **$p < 0.01$, ***$p < 0.001$.

Good biocompatibility is a prerequisite for the application of hydrogels in clinical use. The cytotoxicity of different hydrogels on NIH/3T3 cells was tested by Live/Dead assay. Live/Dead analysis showed that NIH/3T3 cells were viable on GelMA and B–G hydrogels with over 95% viability after being cultured for 5 days (Figure 4C and Figure S2F, Supporting Information). Cells cultured on the hydrogels presented no potential cytotoxicity on the same day according to the ISO 10993-5 standard.[40] Furthermore, the blood compatibility of hydrogel was evaluated by hemolysis assay since the hemolytic rate (HR) is considered to be an important indicator for evaluating biomaterial compatibility.[41] The HR value of all hydrogels is below 2% (Figure 4D), indicating these hydrogels have good blood compatibility.[42] In the gap closure migration experiment (Figure 4E,F), the B–G group showed significant differences in the gap remaining compared to the GelMA group ($p < 0.05$) with the treated time increased from 16 to 32 h.

These results further demonstrated that B–G hydrogel exhibited excellent cytocompatibility, better proliferation and migration, and proper adhesion compared to the BSPMA and GelMA hydrogel groups. Previous works showed that BSP could promote cells (such as human umbilical vascular endothelial cells, fibroblasts, tenocytes) proliferation or migration in vitro and exert positive effects on the MEK/ERK1/2 and PI3K/Akt signaling pathways.[15,43] On the other hand, GelMA can synergistically provide more adherent sites for cells on the hydrogels, thus enabling a better environment for cell adhesion, spreading, and proliferation.[44]

### 2.5. Blood Clotting Studies

Due to common complications such as vascular diseases, anticoagulant therapy to prevent cardiovascular attacks and atherosclerosis is a conventional treatment for diabetic patients.[45] Therefore, a small amount of continuous bleeding after debridement cannot be ignored.[46] Whether it can effectively stop bleeding affects the process of normal wound healing. A mouse hepatic hemorrhage model (**Figure 5**A) was used to evaluate the hemostatic ability of B–G hydrogel. There was a significantly reduced blood loss in B–G-treated group (17.33 ± 3.51 mg) compared with the blank control (152 ± 14.11 mg), and the BSPMA hydrogel and GelMA group also showed different hemostatic ability (36.33 ± 7.02, and 44.33 ± 7.57 mg), respectively (Figure 5B). The hemostatic ability of the hydrogel was further estimated by detecting the clotting time of the blood treated with samples. The blood clotting time of whole blood alone was found to be 6 min (Figure 5C), while a stable clot was formed about 3.5 min after being contacted with BSPMA hydrogel and had no statistical difference with GelMA group.[47] Among these, B–G hydrogel showed the best blood clotting efficacy (≈1.5 min) (Figure 5D). Benefitting from the excellent properties such as porous structure and high swelling rate, B–G hydrogel has the ability to hold a large amount of water or biological liquids. The effectiveness of BSP in promoting PLT aggregation and shape change has been demonstrated in in vivo and in vitro studies.[48] Meanwhile, when fibrinogen and other proteins of blood adsorbed on hydrogel surface, RGD, a signaling peptide, allowed the recognition of the cells' integrin receptors, resulting in the activation of clotting events.[49] Benefitting from the synergistic effect of BSPMA and GelMA, B–G hydrogel shows excellent hemostatic ability.

### 2.6. Wound Healing Study In Vivo

To verify the wound healing efficacy of the B–G hydrogel in vivo, a full-thickness normal and diabetic wound model were established subsequently. As shown in Figure S3A, Supporting Information, B–G hydrogel was applied to the full-thickness (8 mm) acute wounds in ICR mice (a full-thickness normal

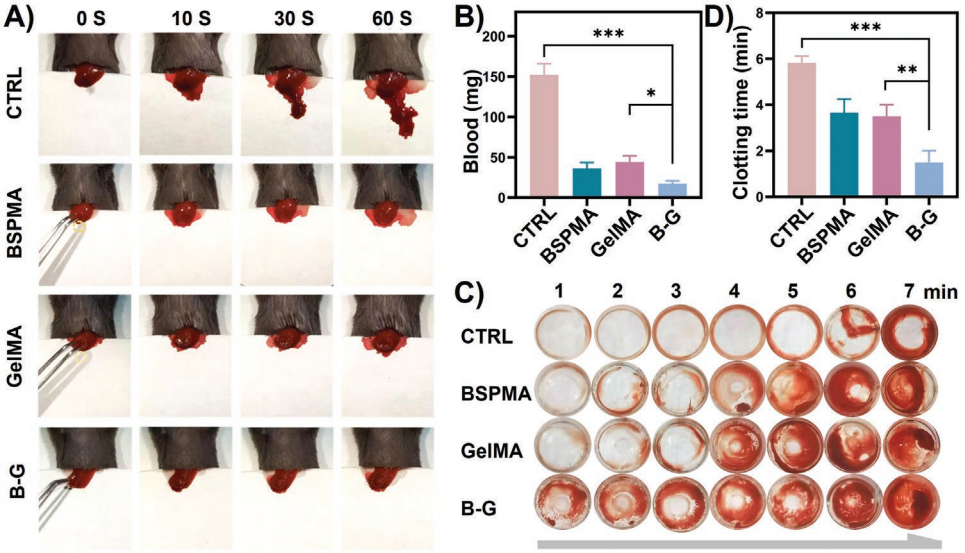


**Figure 5.** A) Representative photographs of hemorrhagic livers treated with control (no treatment), BSPMA, GelMA, and B–G hydrogel at time points of 0, 10, 30 and 60 s. B) Total blood loss from the injured livers treated with control (no treatment), BSPMA, GelMA, and B–G hydrogel ($n = 3$). C) Images of blood clot formed with respect to time under control (no treatment), BSPMA, GelMA, and B–G hydrogel treatments. D) Blood clotting time of each group ($n = 3$). Data represent mean ± SD; $^*p < 0.05$, $^{**}p < 0.01$, $^{***}p < 0.001$.

wound model). According to the digital photos of the wound (Figure S3B, Supporting Information) and the curve diagram (Figure S3C, Supporting Information), the wound size of the BSPMA and B–G groups contracted faster than the control group. As shown in Figure S3D, Supporting Information, the average wound area after BSPMA or B–G treatment was about 70.79% and 73.62% on the 7th day, which was smaller than the control group (≈53.29%). In addition, the average wound healing area of B–G treatment further increased to about 94.98% on the 14th day, while the average wound healing area of GelMA treatment was about 91.25%, indicating that the combination of BSP in GelMA further promoted wound regeneration in vivo. However, there was no significant statistical difference between the BSPMA and B–G groups in wound healing ($p > 0.05$). For chronic wounds (a full-thickness diabetic wound model), the wounds of four groups were recorded at different time points (**Figure 6**A). In Figure 6B, after being treated with B–G hydrogel, the wounds healed faster than other groups, the wound closure rate in BSPMA, GelMA, and B–G hydrogel increased to 33.69 ± 6.98%, 30.34 ± 3.50%, and 43.41 ± 6.74% after 3 days, respectively, which were significantly higher compared with PBS group (20.12 ± 1.71%). In the control group, wound healing was slower in 7 days, and the healing rate did not exceed 50%, owing to the prolonged inflammatory period and the intense inflammatory reaction. In contrast, the B–G group accelerated the wound healing phase transition. With the time increasing, the wounds treated with B–G hydrogel maintained the best healing state among each group. On day 14, the wound healing rate of the B–G group had reached more than 90% (90.57 ± 1.12%); the BSPMA group (82.70 ± 4.22%) and the GelMA group (82.38 ± 1.63%); the control group showed the worst healing ratio (74.39 ± 2.30%). On day 21, the B–G group was almost wholly healed (96.87 ± 1.49%), while the control group still showed a statistically significantly higher unhealed area (85.18 ± 3.69% healed). Quantitative measurement of histological wound cross-sectional length also confirmed this result with the unhealed edge length of the B–G group (815.4 ± 136.4 μm), BSPMA (1251 ± 157.8 μm), GelMA (1330 ± 175.1 μm), and Control (1706 ± 109 μm) (Figure 6C). As presented in Figure 6D, the schematic graph of wound size in different groups presented an apparent change on day 0, 3, 7, 14, and 21.

Re-epithelialization preceded the repair of the dermis and was considered to be the primary step during skin wound healing.[32] It provides an early functional barrier reconstruction for the wound to prevent excessive transdermal water loss and wound infection. To further confirm the wound re-epithelization and granulation tissue formation, we observed the wounds in each group on day 7 and 21. As shown in Figure 6E, the tissue sections of the wounds in the B–G hydrogel group showed relatively complete epithelium. The tissue sections of the wounds administered by the BSPMA and GelMA hydrogels showed incomplete epithelium. However, the wounds treated by the PBS were still in an open state after 7 days. On the 21st day, the B–G hydrogel group had significantly better epithelialization than the control group ($p < 0.001$) (Figure 6F).

Granulation tissue plays a critical role in the regenerative repair process of wound accompanied by inflammation.[50] Therefore, the thicker granulation tissue is a vital indicator to assess the repair effect in the process of wound healing. As shown in Figure 6G, after 21 days, the granulation tissue of the control group was thinner than other hydrogel groups. Among the hydrogel groups, the granulation tissue produced by the B–G hydrogel exhibited a thicker trend than that of BSPMA and GelMA, indicating that the B–G group had the best wound repair effect.

### 2.7. Inflammation and Macrophages Polarization In Vivo

During the wound healing process, inflammation initiates the entire healing cascade and overlaps with the following regeneration phase, which is exceedingly significant to the healing result.[51] F4/80 was selected as an indicator of macrophages, and CD86, CD206, and ARG-1 were used as indicators of M1 and M2 macrophages to assess the level of inflammation changes in diabetic wounds after different treatments. It was shown that on the 3rd day, the M2 macrophage (CD206 or ARG-1) in B–G-treated group was the highest among four groups (Figure S4A–F, Supporting Information). On the 7th day post treatment, immunofluorescence staining of macrophages expressing CD86, CD206, or ARG-1 on the wound surface were shown in **Figure 7**A and Figure S4G, Supporting Information. The CD86 level of the control group was relatively high, and the CD206 or ARG-1 was low (Figure 7B,C and Figure S4H, Supporting Information), indicating that the wound in the control group was still in the inflammatory phase on day 7 and could not transform into the next healing stage. Compared with control groups, the B–G hydrogel group showed a remarkable decrease in CD86 ($p < 0.001$) and increased CD206 or ARG-1 expression ($p < 0.001$). To further verify the effective healing stage transition after B–G hydrogel treatment, the chemokines in wound tissues were measured by enzyme-linked immunosorbent assay (ELISA). As shown in Figure S5A,B, Supporting Information, the pro-inflammatory chemokines TNF-α was much lower in the B–G group (243.5 ± 68.25 pg $mL^{-1}$) compared with the control group (419.2 ± 21.85 pg $mL^{-1}$) ($p < 0.05$). The concentration of IL-10 in the B–G group (745.0 ± 30.64 pg $mL^{-1}$) was higher than that of the control group (558.0 ± 56.53 pg $mL^{-1}$) ($p < 0.05$).

### 2.8. Collagen Deposition and Neovascularization In Vivo

Collagen deposition and vascularization are also crucial for improving ECM formation.[52] Masson's trichrome staining (Figure 7D,E) results indicated that the collagen fibers density in the wound bed was the highest in the B–G hydrogel group in comparison to other groups after 21 days, indicating that the deposition of ECM was remarkably increased in B–G-treated wounds ($p < 0.05$). In addition, after 7 days of treatment, CD31 immunofluorescence staining was applied to evaluate the angiogenesis of diabetic wounds.[53] As shown in Figure 7F, compared with other groups, the expression of CD31 in wounds treated with BSPMA and B–G hydrogel was higher, indicating that more mature capillaries were formed in these two groups. Compared with the control group, the CD31 density of the B–G hydrogel group was significantly increased (Figure 7G). Consistent with these results, the expression of vascular endothelial growth factor (VEGF) in the wound tissues treated with B–G hydrogel was also increased significantly compared

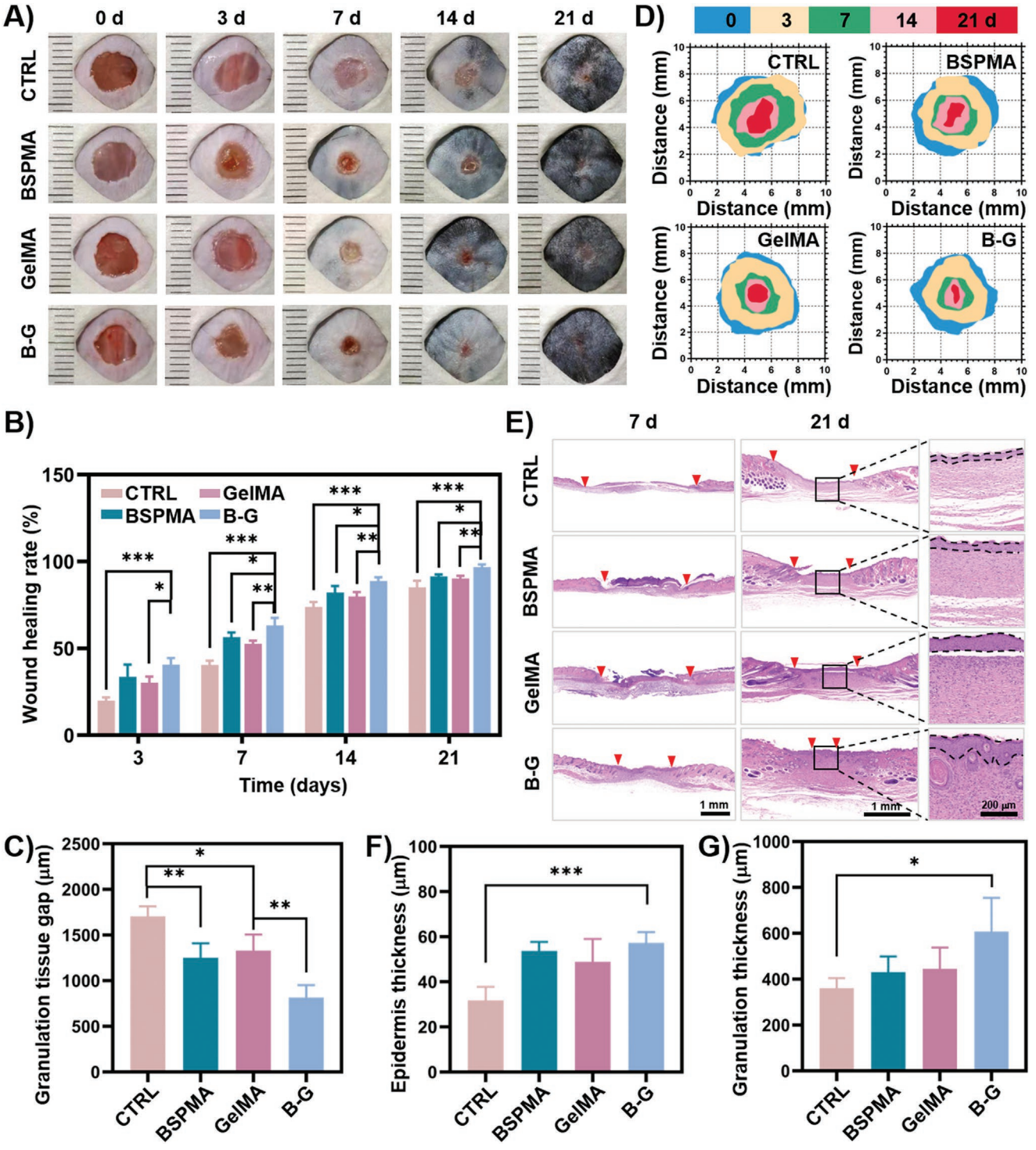


**Figure 6.** A) Representative images of wound healing process in diabetic mice. B) Quantitative data of relative wound area at different time points ($n = 4$). C) Quantification of the cross-sectional length of different wounds at day 21 ($n = 4$). D) Schematic diagram of the wound healed by different treatments during 21 days. E) Representative images of wound tissue sections in different groups stained by H&E on day 7 (Scale bar = 1 mm) and day 21 (Scale bar = 1 mm/200 μm) (The two red arrows represents the unhealed area of the wound). Quantification of F) the epidermis thickness and G) granulation tissue thickness of different wounds ($n = 4$). Data represent mean ± SD; $^{*}p < 0.05$, $^{**}p < 0.01$, $^{***}p < 0.001$.

to the control groups ($p < 0.001$) (Figure S5C, Supporting Information), indicating the advantages of adding BSP-based hydrogel in promoting angiogenesis.[43b,54]

In conclusion, benefitting from the features of individual components and formation of a dual-cross-linked hydrogel network, the B–G hydrogel was conducive to cell adherence,

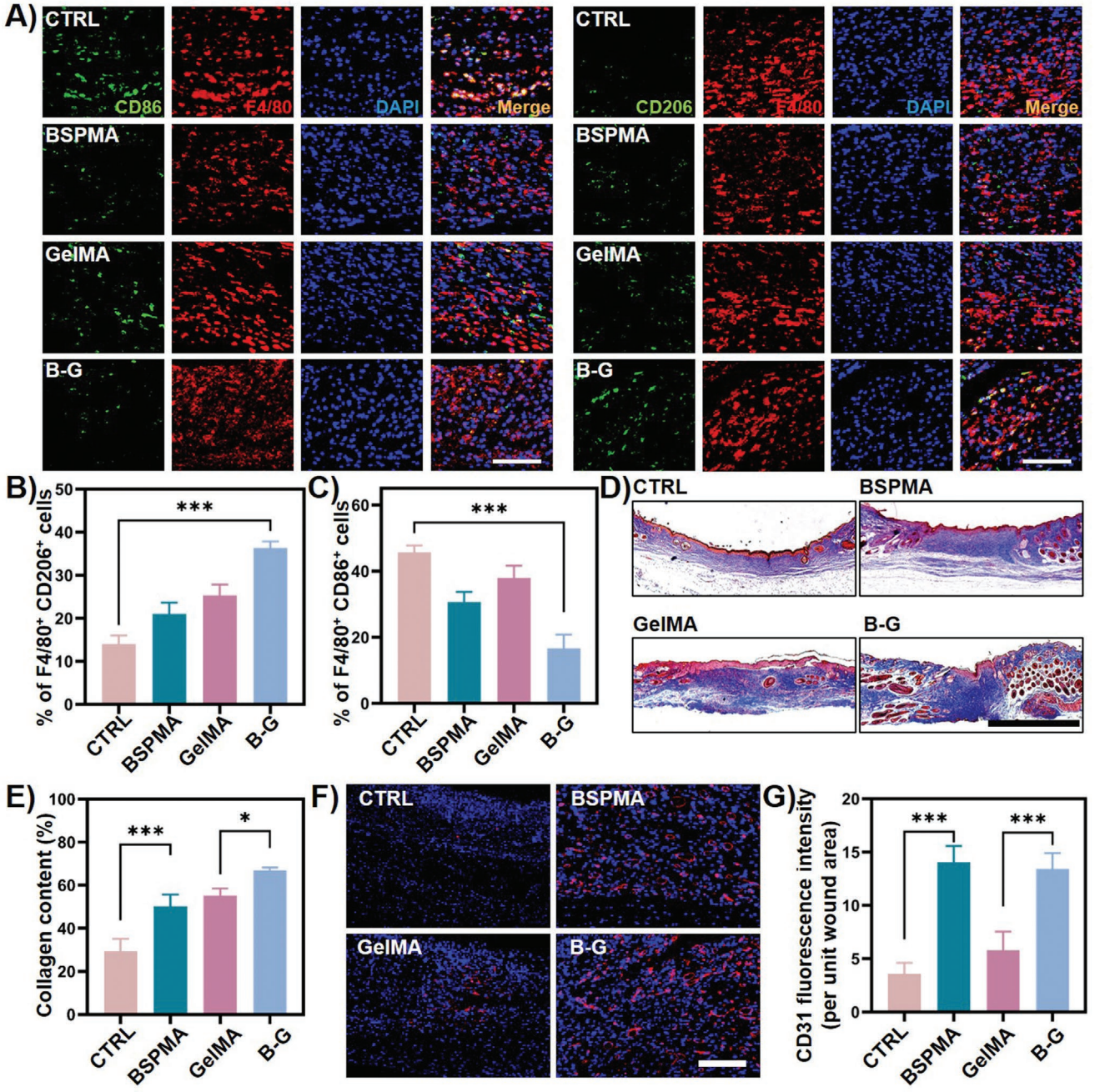


**Figure 7.** A) Immunofluorescent staining of wound bed tissues on day 7 post treatment. M1 phenotype macrophage (CD86, green), M2 phenotype macrophage (CD206, green), F4/80 (red), and nuclei (DAPI, blue) (Scale bar = 100 μm). B) Statistical graph of the percentage of M2 macrophages ($n = 3$). C) Statistical graph of the percentage of M1 macrophages ($n = 3$). D) Masson's trichrome stained sections images of four groups at 21 days post treatment, reflecting collagen deposition (Scale bar = 1 mm). E) Quantification of collagen deposition density in different groups on day 21 ($n = 3$). F) CD31 (red) immunofluorescence staining image on day 7, reflecting neovascularization in wound tissue (Scale bar = 50 μm). G) Statistical data of CD31-positive vessels in wounds ($n = 3$). Data represent mean ± SD; $^*p < 0.05$, $^{**}p < 0.01$, $^{***}p < 0.001$.

proliferation, and differentiation, normalizing the healing process of inflammatory skin defects.

### 2.9. Toxicity of the Hydrogel In Vivo

Finally, we monitored the in vivo toxicity to verify the safety profile of the hydrogel. The blood biochemical parameters on day 7 and hematology parameters on day 21 were evaluated for different hydrogels in mice (Figure S5D, Supporting Information). No significant changes in the blood level of red blood cells (RBCs), white blood cells , PLT, and hemoglobin were observed compared with the control group (diabetic wound model without any treatment). Besides, related indicators of the liver function (glutamic-pyruvic transaminase [ALT] and glutamic oxalacetic transaminase [AST]) and kidney function (blood urea

nitrogen and creatinine) were also tested. The blood level of biochemical indexes showed no apparent toxicity of all hydrogels. Furthermore, after 21 days of treatment, hematoxylin and eosin stain (H&E) staining of the main organs of mice (liver, heart, spleen, lung, and kidney) presented no histopathological changes compared to the control group (Figure S6, Supporting Information). All hydrogel groups are considered to have good safety performance. Previous studies have also shown that GelMA and BSP-based hydrogels have good biocompatibility and can control the rate of degradation by changing their biochemical components and parameters.[12,48b]

## 3. Conclusion

In this study, by incorporating reactive methacrylate groups into BSP, a photocross-linkable BSP prepolymer (BSPMA) was designed. We fabricated a novel hybrid hydrogel (B–G hydrogel) by convenient one-step UV cross-linking. The dual-cross-linked bioactive B–G hydrogel has porous, biodegradable, adjustable mechanical properties and possesses intrinsic dual modulation efficacy to the wound inflammation microenvironment without adding other therapeutic agents. Compared to a single network (GelMA or BSPMA), B–G hydrogel can more efficiently improve the migration, proliferation, and adhesion of NIH/3T3 cells in vitro. Furthermore, in vivo evaluation confirmed the effectiveness of B–G hydrogel in promoting diabetic wound healing by regulating the inflammatory microenvironment. B–G hydrogel can modulate the polarization of macrophages, promote neovascularization, and appropriate collagen deposition in the process of wound healing. Meanwhile, excellent hemostasis and compatibility of B–G hydrogel have also been demonstrated. Taken together, the B–G hydrogel presented a potent ability for chronic wound management and showed promising potential in immunomodulatory-based wound treatments.

## 4. Experimental Section

*Synthesis of GelMA*: Type A gelatin (VETEC, Sigma-Aldrich) was dissolved in PBS at 50 °C to prepare a 10% w/v solution. Then, 8 mL methacrylic anhydride (MA) (M3139, TCI) was slowly added into the gelatin solution drop by drop with continuous stirring for 2 h. After an equivalent amount of PBS was added, the reaction was terminated. The GelMA solution was dialyzed using 8–14 kDa cutoff dialysis tube (MD3534, Yuanye, China) in deionized water for 5 days at 50 °C to remove unreacted MA. After the GelMA solution was frozen for 12 h at −80 °C, it was then lyophilized for further use.

*Synthesis of BSPMA*: Briefly, 1 g BSP (S27914, Yuanye, China) was added in 100 mL distilled water with continuous stirring until fully dissolved. After adding 1 mL MA, the mixture was stirred at 0 °C for 24 h. The pH value of the solution was adjusted between 8 and 10 for 24 h by adding 0.1 N hydrochloric acid or 0.5 M NaOH. Then, it was dialyzed against distilled water for 5 days (MWCO = 3.5 kDa) and lyophilized for 3 days.

*Preparation of BSPMA/GelMA Dual-Cross-Linked (B–G) Hydrogels*: A solution of GelMA and BSPMA was prepared to form the final concentrations of 10% and 2% w/v, respectively. After adding a photoinitiator (Irgacure 2959, 0.5%, w/v), the mixed liquid was irradiated with ultraviolet rays (365 nm UV, 1 w $cm^{-2}$) in the PDMS mold.

*Characterizations of the Hydrogels*: The microstructure of the hydrogels was scanned by SEM (JEM-2100, Japan). The chemical structure of the BSPMA hydrogel was tested by $^1$H-NMR (Bruker, Germany). The mechanical property of the hydrogels was detected by a universal testing machine (INSTRON-5944, USA). The rheology experiments of hydrogels were detected by a rheometer (MARS40, Germany). The swelling and degradation behavior of the hydrogels were evaluated by the swelling ratios (SR) and degradation ratios.

*Microstructure of the Hydrogels*: After spraying a thin gold film on the freeze-dried hydrogel sample, the sample's morphology was observed by SEM (JEM-2100, Japan). The porosity and pore size were measured by ImageJ software.

*Mechanical Property Tests of the Hydrogels*: The premixed solution was completely gelled and made into a cylindrical shape with a height of 4 mm and a diameter of 6 mm. An Instron-5944 mechanical tester was used to compress the samples at a speed of 2 mm $min^{-1}$. The slope of the linear region of the stress–strain curve for 0–10% strain was calculated as the compressive modulus.[55]

*Proton Nuclear Magnetic Resonance*: The degree of functionalization of GelMA and BSPMA was determined by $^1$H-NMR. In short, GelMA was dissolved in $D_2O$ at 15 mg $mL^{-1}$ at 50 °C until completely dissolved. $^1$H-NMR spectroscopy was performed using $^1$H-NMR spectrometer (Bruker, Germany) at room temperature with a frequency of 400 MHz.

*Rheology Property Tests of the Hydrogels*: The hydrogel with a height of 2 mm and a diameter of 8 mm was gently wiped and placed on the platform of the rheometer (MARS40, Germany). In the oscillation amplitude scan, the completely gelled hydrogel was gently wiped off the surface moisture, and the strain amplitude sweep test (CD = 0.01% ~ 30.00%log) was carried out at 20 °C, and the frequency was constant at 1 Hz.

*Molecular Weight Test*: 50 mg sample was placed in a 10 mL volumetric flask and dissolved in mobile phase. The analysis was performed with high-performance gel-filtration chromatography system equipped with 2410 refractive index detector and Empower workstation. The samples were eluted from a Waters ultrahydrogel linear column (Ultrahydrogel Linear 300 mm × 7.8 mm I.D., 40 °C) with a mobile phase of 0.1 N sodium nitrate and a flow rate of 0.5 mL $min^{-1}$. Molecular weights were determined relative to dextran standards: Dextran T-300 (MW300600), DextranT-150 (MW135030), Dextran T-10 (MW9750), and Dextran T-5 (MW2700).

*Swelling Test*: The freeze-dried hydrogel was immersed in 2 mL PBS at room temperature. The hydrogel was collected from the PBS at each predetermined time interval, and excess fluid was removed with the filter paper. The calculation formula of SR was as follows: $SR = (W_t - W_0)/W_0 \times 100\%$. $W_0$ and $W_t$ were the initial weight of the hydrogel after freeze-drying and the weight after swelling, respectively.

*Degradation Test*: To test the degradation of hydrogels in vitro,[32] an equal volume of the hydrogel blocks were immersed in a 24-well plate with 1.5 mL PBS containing 1.25 U $mL^{-1}$ type II collagenase (C909788, Macklin) at 37 °C for 21 days, and the medium was refreshed every 3 days to keep enzyme activity. At each time point, the hydrogel samples were rinsed with deionized water, excess fluid was removed with filter paper, and then freeze-dried for 3 days.

The degradation ratio of the hydrogel was calculated as follows: the degradation ratio (%) = $(W_0 - W_t)/W_0 \times 100\%$. $W_t$ stood for the weight of the remaining hydrogel at each time point, and $W_0$ stood for the initial weight of the hydrogel.

*Assessment of Macrophages Polarization In Vitro*: To evaluate the effect of B–G hydrogel on the polarization of macrophages, Raw 264.7 macrophages were cocultured with BSPMA, GelMA, and B–G hydrogels, respectively. In short, after incubated for 24 h, the RAW 264.7 cells (ATCC) were cultured with medium containing 1 μg $mL^{-1}$ LPS (L2880, Sigma) for 15 h. Then, the culture medium was removed. After rinsing gently with PBS twice, cells were added into hydrogel-coated 6-well plates at the density of $5 \times 10^4$ cells per well and cultured continuously for 4 days. 40 ng $mL^{-1}$ IL-4-treated group was used as the positive control. Cells treated with LPS alone were used as the negative control.

*Flow Cytometry*: To evaluate the effect of hydrogels on the polarization of macrophages, flow cytometry was applied to detect the CD86 and

CD206 expression of Raw 264.7 cells cultured in different hydrogels. After being treated with LPS and different hydrogels, $1 \times 10^6$ cells were collected and incubated with 100 µL PBS containing CD86/FITC (CD86 [B7-2] monoclonal, eBioscience) antibody for 0.5 h at 4 °C and CD206/APC (CD206 [MMR] Monoclonal, eBioscience) antibody for 1 h at room temperature for flow cytometry assay (FACS Aria Fusion, BD). Data were analyzed by Flowjo Analysis Software.

*Quantitative Polymerase Chain Reaction*: q-PCR was carried out to test the influences of BSPMA, GelMA, and B–G hydrogels on the gene expressions of TNF-α, IL-10, IL-6, and TGF-β in RAW 264.7 cells.[56] After administration, the RAW 264.7 cells were gently washed with PBS and incubated with 1 mL TRIzol reagent (R0016, Beyotime) on ice for 10–15 min. 200 µL chloroform was added to the collected total cell lysate and left for 10 min. After centrifugation, 500 µL isopropanol was added to the supernatant for 10 min. Then, the precipitate was washed twice with 75% anhydrous ethanol and air-dried before adding DEPC solution. Finally, pure RNA was obtained, which was quantified with a trace ultraviolet spectrophotometer (Nano Drop ONE, Thermo). cDNA was synthesized by Hifair III 1st Strand cDNA Synthesis SuperMix (Yeasen), and q-PCR was conducted by Hieff qPCR SYBR Green Master Mix (Yeasen). The $2^{-\Delta\Delta Ct}$ method was employed to analyze the relative gene expression. The primer sequences are listed in Table S1, Supporting Information.

*Cell Proliferation Assessment*: Cell Counting Kit-8 (CCK-8) (C0038, Beyotime) was used to detect cell proliferation. 4 µL of gel per well was cross-linked on the bottom of a 96-well plate, subsequently, NIH/3T3 cells with a density of 2000 cells per well were cultured in the plate. On day 1, 3, and 5, CCK-8 was added to follow the kit protocol. After incubation, the absorbance at 450 nm was detected by a microplate reader (Synergy H1). The cell proliferation = $(OD_t - OD_a)/(OD_c - OD_b)$. $OD_t$ represented the experimental group, $OD_a$ represented the blank group with the corresponding hydrogel only, $OD_c$ represented the control group, and $OD_b$ represented the blank group.

*Cell Migration Assessment*: To study the effect of hydrogel on the migration of fibroblasts, a scratch experiment was performed. $2 \times 10^6$ cells per well NIH/3T3 cells were cultured in GelMA or B–G hydrogel coated 6-well plate for 24 h. After removing the medium, a scratch was made with the same width on the bottom of each well. After incubating for a certain time, the cells were observed by an inverted microscope (DMI8, Lecia), and images were taken to monitor the migration of the cells on the scratched area.

*Cell Adhesion Assessment*: Briefly,[57] under aseptic conditions, 25 µL hydrogel were cross-linked on the bottom of a 24-well plate, then $3 \times 10^5$ cells were seeded on the gel and were cultured for 4 h. The same number of cells was directly seeded on the surface of a 24-well TCP cell culture dish as a positive control. The medium was gently aspirated from the well after 4 h, and then cells were gently rinsed twice with PBS. After being stained by DAPI dye for 5 min, the cells were observed under an inverted microscope (DMI8, Lecia).

*Evaluation Cytocompatibility of the Hydrogels*: The cytotoxicity of the hydrogels was evaluated by Live/Dead assay. For Live/Dead testing, 25 µL of hydrogel was spread on the bottom of a 24-well plate, and then 15 000 fibroblast suspension was added. After being cultured for 1, 3, and 5 days, the hydrogel was gently washed with PBS and then incubated with Live/Dead Detection Kit (L6037, UE) according to the protocol. The cells were observed under an inverted microscope.

*Hemocompatibility of the Hydrogels*: The hemocompatibility of hydrogels was investigated by a hemolysis assay.[41] Fresh mouse blood was centrifuged at 2000 rpm for 10 min to isolate RBCs and then washed with 0.9% NaCl solution for three times. Purified RBCs were diluted with 0.9% NaCl to obtain RBC suspension (5%, v/v). 200 µL of the RBCs suspension mixed with 800 µL of 0.9% NaCl solution was prepared as a negative control; 200 µL of the RBCs suspension mixed with 800 µL of 0.1% Triton X-100 (T8200, Solarbio) was prepared as a positive control; 200 µL of the RBCs suspension mixed with 100 µL of BSPMA, GelMA, or B–G hydrogels and 700 µL of 0.9% NaCl solution was prepared as the experimental group. After being incubated at 37 °C for 2 h, the mixture in the tubes were centrifuged and captured by a digital camera. The absorbance of the supernatant measured by a microplate reader at 540 nm was used to calculate the HR. HR (%) = $[(A_h - A_n)/(A_t - A_n)] \times 100\%$. $A_h$, $A_t$, and $A_n$ stood for the absorbance of each sample, positive control, and negative control at 540 nm, respectively.

*Blood Clotting Effect of the Hydrogels*: The blood clotting efficacy of the hydrogels in vitro was evaluated according to the blood clotting method.[58] The hydrogels were placed into a 96-well plate and kept in the warm water bath at 37 °C for 10 min followed by adding anticoagulated fresh mouse blood (45 µL) and then 9 µL $CaCl_2$ (25 mmol $L^{-1}$) at different time points. The uncoagulated blood was carefully sucked away and gently washed twice with 0.9% NaCl solution. Then, blood clots were observed.

Liver hemorrhaging mice (C57BL/6, 20–25 g, male) were used to evaluate the hemostatic potential of the B–G hydrogels in vivo. All animal breeding and operations were approved by the Animal Ethics Committee of Nanjing University of Chinese Medicine (202011A034). Mice in each group were anesthetized and fixed to the 30° slanted operating board. After sterilizing the abdominal skin with alcohol, the liver was carefully exposed with surgical scissors. The preweighing filter paper was put under the liver. A 3 mm diameter wound was made in the liver with a No. 20 needle, and then quickly covered with hydrogel. Digital images were captured at 0, 10, 30, and 60 s, and finally, the filter papers were weighed.

*Wound Healing Assessment*: The female ICR mice and male C57BL/6 mice were purchased from the Nanjing Qinglongshan Experimental Animal Technology and the Beijing Weitong Lihua Experimental Animal Technology, respectively. All animals were housed in SPF-level animal facilities, with a 12-h cycle of alternating light and dark rhythms.

For diabetic wound healing assessment, Male C57BL/6 mice were given a high-fat feed and were intraperitoneally injected 100 mg $kg^{-1}$ streptozotocin (STZ, S8050, Solarbio) in citric acid-sodium citrate buffer once a day for 2 days to induce diabetic models. 2 weeks post STZ injection, the mice with blood glucose exceeding 16.8 mmol $L^{-1}$ were considered diabetic.[59] In order to evaluate the wound healing effect, C57BL/6 diabetic mice were anesthetized, and 6 mm diameter full-thickness skin wounds were created by the skin biopsy punches on the shaved and sterilized dorsum. Then, 50 µL each of BSPMA, GelMA, and B–G hydrogels were cross-linked in vitro by ultraviolet light for 15 s into thin discs, and washed gently with PBS to remove impurities. The animals were randomly divided into four groups and were applied with PBS (Control), BSPMA hydrogel, GelMA hydrogel, and B–G hydrogel, respectively. Digital images of the wounds were captured at 3, 7, 14, and 21 days after the operation and measured with ImageJ software. The percentage of unhealed area = $[A_{(3,\ 7,\ 14,\ 21)}/A_0] \times 100\%$. $A_0$ and $A_{(3,\ 7,\ 14,\ 21)}$ stood for the unhealed areas on day 0 and day 3, 7, 14, and 21, respectively.

For normal wound healing assessment, after ICR mice were anesthetized, 8 mm diameter full-thickness skin wounds were created by the skin biopsy punches on the shaved and sterilized dorsum. The ICR mice were randomly divided into four groups and applied PBS (Control), BSPMA hydrogel, GelMA hydrogel, and B–G hydrogel, respectively. Digital images of the wound were captured at 3, 7, and 14 days after the operation and measured with ImageJ software. The percentage of unhealed area = $[A_{(3,\ 7,\ 14)}/A_0] \times 100\%$, where $A_0$ and $A_{(3,\ 7,\ 14)}$ stood for the unhealed areas on day 0 and day 3, 7, and 14, respectively.

*Histological and Immunofluorescent Analysis*: On day 3, 7, and day 21 post administration, the regenerated dorsal skins were collected. After being fixed with 4% w/v paraformaldehyde solution, the tissues were embedded in molten paraffin for next-step staining.

*H&E Staining*: The sections were deparaffinized in xylene for 20 min, and then washed with ethanol gradient solution (100%, 95%, 80%, and 75%). After gently absorbing the water, immerse the slices in hematoxylin for 5 min, and rinse with running water. The sections were then immersed in eosin staining for 2 min, then dehydrated in absolute ethanol, and get transparent in xylene for 15 min. Finally, the slides were sealed and preserved with neutral resin. A Nikon microscope (Nikon, Tokyo, Japan) was used to observe the stained sections and collect

images while measuring the thickness of granulation and epidermis. The cross section of the tissue wound was measured by the scanner (Pannoramic DESK, P-MIDI, P250).

*Masson Staining*: The steps of deparaffinization and rehydration of the sections were the same as the above H&E staining. The Masson Tricolor Staining Kit was used for staining. In short, the slides were stained with iron hematoxylin according to the manufacturer's instructions. After rinsing with running water, and immersing in the differentiation solution for 5 s, the fibrous tissue was stained with Ponceau acid fuchsin solution for 5 min, immersed in a phosphomolybdic acid solution for 1 min, and stained with aniline blue for 4 min. The sections were differentiated with 1% glacial acetic acid, dehydrated, mounted, and covered. The steps were the same as H&E staining. The scanner (Pannoramic DESK, P-MIDI, P250) was used for image acquisition and ImageJ software was used for analysis and measurement.

*ELISA Test*: Fresh skin wound tissue of diabetic mice was washed in precooled PBS to remove blood or impurities, placed on filter paper to absorb water, and cut 30 mg skin tissue for measurement. Subsequently, the weighed tissue was cut into pieces in cold PBS and homogenized, and then centrifuged at 12 000 rpm for 10 min at 4 °C for supernatant collection. TNF-α, IL-10, and VEGF concentrations were measured with ELISA kit (Jeb-202011, Nanjing Jin Yibai Biological Technology Co. Ltd.). All procedures were performed according to the manufacturer's instructions.

*Immunofluorescent Staining*: For in vitro immunofluorescence staining, cells were fixed with 4% paraformaldehyde for 10 min. After centrifugation, resuspend them with PBS and dropped the cells on the adhesive slide. After drying, 0.3% Triton X-100 was added at room temperature for 20 min. After washing three times, 3% BSA was added dropwise to the cells at room temperature for 1 h. After the primary antibody incubation overnight, the secondary antibody and antifluorescence quencher (including DAPI) were added dropwise under dark conditions, and images were collected on a confocal microscope (TCS SP8, Leica).

For in vivo immunofluorescence, after deparaffinization, hydration, and antigen retrieval, the skin tissue sections were treated for 30 min at room temperature with 0.3% PBST, washed three times with PBS, and blocked with 5% BSA at room temperature for 1 h. The sections were incubated with CD206 (1:400, GB113497, Servicebio), CD86 (1:100, GB13585, Servicebio), ARG-1 (1:00, BM4000, Boster Biological Technology), F4/80 (1:100, 123101, Biolegend), or CD31 (1:200, GB11063-2, Servicebio) (dissolved in 1% BSA) at 4 °C overnight. After washing with PBS, secondary antibodies (Servicebio) diluted in PBS were added and incubated at 37 °C for 60 min. Finally, an appropriate amount of antifluorescence quenching agent (including DAPI) was added dropwise and incubated for 10 min, and fluorescent images of the slices were taken using a fluorescence microscope.

*Toxicity of the Hydrogels*: After 7 or 21 days, 1.5 mL of mice blood was harvested for hematological monitoring. On day 21, the main organs (liver, kidney, spleen, heart, and lung) of the animals were collected after euthanasia. H&E staining slides were prepared and subsequently observed by an optical microscope (DM2500, Leica).

*Statistical Analysis*: The statistical analysis was carried out using Prism 8.0. Data were presented as mean ± SD. Student *t*-test or one/two-way ANOVA was performed to determine statistical significance. *p* value less than 0.05 was regarded as statistical significance.

## Supporting Information

Supporting Information is available from the Wiley Online Library or from the author.

## Acknowledgements

This research was funded by National Natural Science Foundation of China (No. 81703940), the Natural Science Foundation of Nanjing University of Chinese Medicine (No. NZY81703940), and the Priority Academic Program Development of Jiangsu Higher Education Institutions (Nursing, 2019YSHL019), and was also sponsored by Qing Lan Project of Jiangsu Province (2021).

## Conflict of Interest

The authors declare no conflict of interest.

## Author Contributions

J.L., M.Q., and C.W. contributed equally to this work. X.Z., G.X., and X.J. conceived the project, designed the studies. J.L., M.Q., C.W., Y.X., and H.H. carried out the experiments and analyzed the results. X.Z., G.X., X.J., Q.C., and W.S. revised the manuscript. X.Z., G.X., and X.J. supervised the project.

## Data Availability Statement

The data that support the findings of this study are available from the corresponding author upon reasonable request.

## Keywords

dual-cross-linked hydrogels, inflammation modulation, wound healing

Received: October 10, 2021
Revised: January 9, 2022
Published online: March 23, 2022

[1] A. Rastogi, G. Goyal, R. Kesavan, A. Bal, H. Kumar, Mangalanadanam, P. Kamath, E. B. Jude, D. G. Armstrong, A. Bhansali, *Diabetes Res. Clin. Pract.* **2020**, *162*, 108113.
[2] Z. Xu, B. Liang, J. Tian, J. Wu, *Biomater. Sci.* **2021**, *9*, 4388.
[3] H. Wang, Z. Xu, M. Zhao, G. Liu, J. Wu, *Biomater. Sci.* **2021**, *9*, 1530.
[4] M. Kloc, R. M. Ghobrial, J. Wosik, A. Lewicka, S. Lewicki, J. Z. Kubiak, *J. Tissue Eng. Regener. Med.* **2019**, *13*, 99.
[5] G. V. Ganesh, K. M. Ramkumar, *Inflammation Res.* **2020**, *69*, 347.
[6] M. Hesketh, K. Sahin, Z. West, R. Murray, *Int. J. Mol. Sci.* **2017**, *18*, 1545.
[7] Z. Feng, Q. Su, C. Zhang, P. Huang, H. Song, A. Dong, D. Kong, W. Wang, *Adv. Funct. Mater.* **2020**, *30*, 2006454.
[8] Y. Feng, Q. Li, D. Wu, Y. Niu, C. Yang, L. Dong, C. Wang, *Biomaterials* **2017**, *134*, 128.
[9] Q. Li, Y. Niu, P. Xing, C. Wang, *Chin. Med.* **2018**, *13*, 7.
[10] D. Xu, Y. Pan, J. Chen, *Front. Pharmacol.* **2019**, *10*, 1168.
[11] Y. Wang, J. Liu, Q. Li, Y. Wang, C. Wang, *Biotechnol. Lett.* **2015**, *37*, 1.
[12] Y. Niu, Q. Li, R. Xie, S. Liu, R. Wang, P. Xing, Y. Shi, Y. Wang, L. Dong, C. Wang, *Biomaterials* **2017**, *139*, 39.
[13] Y. Zhao, Q. Wang, S. Yan, J. Zhou, L. Huang, H. Zhu, F. Ye, Y. Zhang, L. Chen, L. Chen, T. Zheng, *Front. Pharmacol.* **2021**, *12*, 659215.
[14] a) L. Yue, W. Wang, Y. Wang, T. Du, W. Shen, H. Tang, Y. Wang, H. Yin, *Int. J. Biol. Macromol.* **2016**, *89*, 376; b) L. Luo, Y. Q. Liu, X. Cai, Y. Wang, J. Xue, J. Zhang, F. Yang, *Saudi J. Gastroenterol.* **2019**, *25*, 302.
[15] C. Zhang, Y. He, Z. Chen, J. Shi, Y. Qu, J. Zhang, *Evidence-Based Complementary Altern. Med.* **2019**, *2019*, 9212314.

[16] K. Yue, G. Trujillo-de Santiago, M. M. Alvarez, A. Tamayol, N. Annabi, A. Khademhosseini, *Biomaterials* **2015**, *73*, 254.
[17] Z. Ahmadian, A. Correia, M. Hasany, P. Figueiredo, F. Dobakhti, M. R. Eskandari, S. H. Hosseini, R. Abiri, S. Khorshid, J. Hirvonen, H. A. Santos, M. A. Shahbazi, *Adv. Healthcare Mater.* **2021**, *10*, 2001122.
[18] B. H. Cha, S. R. Shin, J. Leijten, Y. C. Li, S. Singh, J. C. Liu, N. Annabi, R. Abdi, M. R. Dokmeci, N. E. Vrana, A. M. Ghaemmaghami, A. Khademhosseini, *Adv. Healthcare Mater.* **2017**, *6*, 1700289.
[19] A. Gaspar-Pintiliescu, A. M. Stanciuc, O. Craciunescu, *Int. J. Biol. Macromol.* **2019**, *138*, 854.
[20] H. Hu, F. J. Xu, *Biomater. Sci.* **2020**, *8*, 2084.
[21] Z. Chen, L. Cheng, Y. He, X. Wei, *Int. J. Biol. Macromol.* **2018**, *120*, 2076.
[22] M. H. M. Oudshoorn, R. Rissmann, J. A. Bouwstra, W. E. Hennink, *Polymer* **2007**, *48*, 1915.
[23] J. W. Nichol, S. T. Koshy, H. Bae, C. M. Hwang, S. Yamanlar, A. Khademhosseini, *Biomaterials* **2010**, *31*, 5536.
[24] X. Zhou, Z. Luo, A. Baidya, H. Kim, C. Wang, X. Jiang, M. Qu, J. Zhu, L. Ren, F. Vajhadin, P. Tebon, N. Zhang, Y. Xue, Y. Feng, C. Xue, Y. Chen, K. Lee, J. Lee, S. Zhang, C. Xu, N. Ashammakhi, S. Ahadian, M. Dokmeci, Z. Gu, W. Sun, A. Khademhosseini, *Adv. Healthcare Mater.* **2020**, *9*, 2000527.
[25] a) J. Huang, L. Chen, Z. Gu, J. Wu, *J. Biomed. Nanotechnol.* **2019**, *15*, 1357; b) C. H. Lin, J. J. Su, S. Y. Lee, Y. M. Lin, *J. Tissue Eng. Regener. Med.* **2018**, *12*, 2099; c) X. Zhang, J. Li, P. Ye, G. Gao, K. Hubbell, X. Cui, *Acta Biomater.* **2017**, *59*, 317.
[26] Z. Li, K. M. Bratlie, *Macromol. Biosci.* **2021**, *21*, 2100031.
[27] a) S. Jiang, S. C. Li, C. Huang, B. P. Chan, Y. Du, *Adv. Healthcare Mater.* **2018**, *7*, 1700894; b) F. J. O'Brien, B. A. Harley, I. V. Yannas, L. J. Gibson, *Biomaterials* **2005**, *26*, 433.
[28] N. Annabi, D. Rana, E. S. Sani, R. Portillo-Lara, J. L. Gifford, M. M. Fares, S. M. Mithieux, A. S. Weiss, *Biomaterials* **2017**, *139*, 229.
[29] a) C. Li, G. Guan, R. Reif, Z. Huang, R. K. Wang, *J. R. Soc., Interface* **2012**, *9*, 831; b) B. Saleh, H. K. Dhaliwal, R. Portillo-Lara, E. S. Sani, R. Abdi, M. M. Amiji, N. Annabi, *Small* **2019**, *15*, 1902232.
[30] L. Yan, K. Han, B. Pang, H. Jin, X. Zhao, X. Xu, C. Jiang, N. Cui, T. Lu, J. Shi, *Chem. Eng. J.* **2021**, *414*, 128836.
[31] B. C. Nwomeh, H. X. Liang, I. K. Cohen, D. R. Yager, *J. Surg. Res.* **1999**, *81*, 189.
[32] X. Zhao, Q. Lang, L. Yildirimer, Z. Y. Lin, W. Cui, N. Annabi, K. W. Ng, M. R. Dokmeci, A. M. Ghaemmaghami, A. Khademhosseini, *Adv. Healthcare Mater.* **2016**, *5*, 108.
[33] Q. Zhang, C. Chang, C. Qian, W. Xiao, H. Zhu, J. Guo, Z. Meng, W. Cui, Z. Ge, *Acta Biomater.* **2021**, *125*, 197.
[34] A. T. Rowley, R. R. Nagalla, S. W. Wang, W. F. Liu, *Adv. Healthcare Mater.* **2019**, *8*, 1801578.
[35] W. Liu, M. Wang, W. Cheng, W. Niu, M. Chen, M. Luo, C. Xie, T. Leng, L. Zhang, B. Lei, *Bioact. Mater.* **2021**, *6*, 721.
[36] J. Gan, C. Liu, H. Li, S. Wang, Z. Wang, Z. Kang, Z. Huang, J. Zhang, C. Wang, D. Lv, L. Dong, *Biomaterials* **2019**, *219*, 119340.
[37] M. F. Siqueira, J. Li, L. Chehab, T. Desta, T. Chino, N. Krothpali, Y. Behl, M. Alikhani, J. Yang, C. Braasch, D. T. Graves, *Diabetologia* **2010**, *53*, 378.
[38] A. R. Donaldson, C. E. Tanase, D. Awuah, P. V. Bathrinarayanan, L. Hall, M. Nikkhah, A. Khademhosseini, F. Rose, C. Alexander, A. M. Ghaemmaghami, *Front. Bioeng. Biotechnol.* **2018**, *6*, 116.
[39] S. Cai, C. Wu, W. Yang, W. Liang, H. Yu, L. Liu, *Nanotechnol. Rev.* **2020**, *9*, 971.
[40] M. A. Al Enezy-Ulbrich, H. Malyaran, R. D. Lange, N. Labude, R. Plum, S. Rütten, N. Terefenko, S. Wein, S. Neuss, A. Pich, *Adv. Funct. Mater.* **2020**, *30*, 2003528.
[41] Y. Liang, X. Zhao, T. Hu, B. Chen, Z. Yin, P. X. Ma, B. Guo, *Small* **2019**, *15*, 1900046.
[42] L. Mao, L. Wang, M. Zhang, M. W. Ullah, L. Liu, W. Zhao, Y. Li, A. A. Q. Ahmed, H. Cheng, Z. Shi, G. Yang, *Adv. Healthcare Mater.* **2021**, *10*, 2100402.
[43] a) Z. Y. Chen, S. H. Chen, C. H. Chen, P. Y. Chou, C. C. Yang, F. H. Lin, *Polymers* **2020**, *12*, 2567; b) C. Wang, J. Sun, Y. Luo, W. Xue, H. Diao, L. Dong, J. Chen, J. Zhang, *Biotechnol. Lett.* **2006**, *28*, 539.
[44] M. Sun, X. Sun, Z. Wang, S. Guo, G. Yu, H. Yang, *Polymers* **2018**, *10*, 12920.
[45] M. A. Creager, T. F. Luscher, F. Cosentino, J. A. Beckman, *Circulation* **2003**, *108*, 1527.
[46] Y. G. Hwang, J. W. Lee, E. A. Won, S. H. Han, *J. Diabetes Res.* **2019**, *2019*, 9316380.
[47] N. Rajabi, M. Kharaziha, R. Emadi, A. Zarrabi, H. Mokhtari, S. Salehi, *J. Colloid Interface Sci.* **2020**, *564*, 155.
[48] a) L. Dong, X. X. Liu, S. X. Wu, Y. Mei, M. J. Liu, Y. X. Dong, J. Y. Huang, Y. J. Li, Y. Huang, Y. L. Wang, S. G. Liao, *Biomed. Pharmacother.* **2020**, *130*, 110537; b) Q. Zhang, C. Qi, H. Wang, X. Xiao, Y. Zhuang, S. Gu, Y. Zhou, L. Wang, H. Yang, W. Xu, *Carbohydr. Polym.* **2019**, *226*, 115304.
[49] a) S. Pourshahrestani, E. Zeimaran, N. A. Kadri, N. Mutlu, A. R. Boccaccini, *Adv. Healthcare Mater.* **2020**, *9*, 2000905; b) Z. Zhai, K. Xu, L. Mei, C. Wu, J. Liu, Z. Liu, L. Wan, W. Zhong, *Soft Matter* **2019**, *15*, 8603.
[50] J. Qu, X. Zhao, Y. Liang, T. Zhang, P. X. Ma, B. Guo, *Biomaterials* **2018**, *183*, 185.
[51] S. Nour, N. Baheiraei, R. Imani, M. Khodaei, A. Alizadeh, N. Rabiee, S. M. Moazzeni, *J. Mater. Sci.: Mater. Med.* **2019**, *30*, 120.
[52] S. Patel, S. Srivastava, M. R. Singh, D. Singh, *Biomed. Pharmacother.* **2019**, *112*, 108615.
[53] a) Y. Zhu, Z. Ma, L. Kong, Y. He, H. F. Chan, H. Li, *Biomaterials* **2020**, *256*, 120216; b) J. Wu, A. Chen, Y. Zhou, S. Zheng, Y. Yang, Y. An, K. Xu, H. He, J. Kang, J. A. Luckanagul, M. Xian, J. Xiao, Q. Wang, *Biomaterials* **2019**, *222*, 119398.
[54] Y. Huang, F. Shi, L. Wang, Y. Yang, B. M. Khan, K. L. Cheong, Y. Liu, *Int. J. Biol. Macromol.* **2019**, *132*, 729.
[55] W. Xiao, J. He, J. W. Nichol, L. Wang, C. B. Hutson, B. Wang, Y. Du, H. Fan, A. Khademhosseini, *Acta Biomater.* **2011**, *7*, 2384.
[56] L. Kong, Z. Wu, H. Zhao, H. Cui, J. Shen, J. Chang, H. Li, Y. He, *ACS Appl. Mater. Interfaces* **2018**, *10*, 30103.
[57] F. Wang, Y. Wang, C. Tian, S. Xu, R. Wang, K. Hou, W. Chen, P. Zhao, L. Yu, Z. Lu, D. L. Kaplan, Q. Xia, *Acta Biomater.* **2018**, *79*, 239.
[58] N. S. M. Pillai, K. Eswar, S. Amirthalingam, U. Mony, P. K. Varma, *ACS Appl. Bio Mater.* **2019**, *2*, 865.
[59] Z. Tu, M. Chen, M. Wang, Z. Shao, X. Jiang, K. Wang, Z. Yao, S. Yang, X. Zhang, W. Gao, C. Lin, B. Lei, C. Mao, *Adv. Funct. Mater.* **2021**, *31*, 2100924.